

YBa₂Cu₃O₇ Josephson diode operating as a high-efficiency ratchet

Christoph Schmid,^{*} Alireza Jozani,^{*} Reinhold Kleiner, Dieter Koelle, and Edward Goldobin[†]

*Physikalisches Institut, Center for Quantum Science (CQ) and LISA⁺,
Universität Tübingen, Auf der Morgenstelle 14, D-72076 Tübingen, Germany*

(Dated: August 6, 2024 File: **He-FIB-Ratchet***v19.T_EX)

Using a focused He⁺ beam for nanopatterning and writing of Josephson barriers we fabricated specially shaped Josephson junctions of in-line geometry in YBa₂Cu₃O₇ thin film microbridges with an asymmetry ratio of critical currents of opposite polarities (non-reciprocity ratio) ≈ 7 at optimum magnetic field. Those *Josephson diodes* were subsequently used as ratchets to rectify an applied ac current into a dc voltage. We also demonstrate the operation of such a ratchet in the loaded regime, where it produces a nonzero dc output power and yields a thermodynamic efficiency of up to 75%. The ratchet shows record figures of merit: an output dc voltage of up to 212 μ V and an output power of up to 0.2 nW. The device has an essential area $\approx 1 \mu\text{m}^2$. For rectification of quasistatic Gaussian noise, the figures of merit are more modest, however the efficiency can be as high as for the deterministic ac drives within some regimes. Since the device is based on YBa₂Cu₃O₇, it can operate at temperatures up to ~ 40 K, where more noise is available for rectification.

Keywords: He-FIB, Josephson junction, Josephson ratchet, Josephson diode, YBCO

I. INTRODUCTION

Ratchets, also known as Brownian motors, received a lot of attention two decades ago [1–3] stimulated by the investigation of molecular motors in biological systems in the 1990s [4, 5]. In the simplest model one can imagine a point-like particle moving in one dimension along an asymmetric periodic potential under the action of a deterministic or random applied force (drive) with zero time-average. The ultimate goal of this device is to rectify the applied force and produce a directed motion of the particle (net transport). Possible applications range from rectification or mixing of electric signals to the mechanical separation of various (nano-)particles (*e.g.*, viruses) [1, 6]. A lot of different designs were investigated including asymmetric rocking and flashing potentials, asymmetric and random (noisy) drives with different spectral properties, *etc.* [2, 3]. However we would like to remind right away that rectification of equilibrium thermal fluctuations (white noise) is forbidden by the second law of thermodynamics [7]. Still, it is of basic interest to study how close one can approach this limit and still rectify, and which ingredients in terms of noise parameters, bandwidth, *etc.* are essential.

Among different realizations of ratchets one of the interesting classes includes Josephson ratchets (JRs). They have a number of advantages[8, 9]: (i) directed motion (of the Josephson phase) results in an average dc voltage \bar{V} (via the second Josephson relation), which is easily detected experimentally; (ii) Josephson junctions (JJs) are very fast devices, which can operate (capture and rectify deterministic or stochastic drives) in a broad frequency range from dc up to few hundred GHz, capturing a lot of spectral energy in the quasistatic regime; (iii) by

varying the junction design and bath temperature, both overdamped and underdamped regimes are accessible.

In a JR the applied bias current I plays the role of a force acting on the system. Different realizations of JRs were demonstrated, including superconducting quantum interference device (SQUID) ratchets[10–15], Josephson vortex ratchets based on annular long Josephson junctions (ALJJs)[8, 9, 16, 17] or Josephson junction arrays (JJA)[18–21], or tunable φ -JJ ratchets[22]. The key parameter that determines the figures of merit in JRs is the asymmetry of the potential. It is defined as the ratio of its maximum slopes (that define depinning forces) for the motion of the particle in the positive and the negative directions. In Josephson junctions this is equal to the ratio of positive and negative critical currents I_{c+} and I_{c-} , respectively. We define the asymmetry \mathcal{A} as a quantity that is positive and larger than 1, *i.e.*,

$$\mathcal{A} = \begin{cases} |I_{c-}|/I_{c+}, & \text{if } I_{c+} < |I_{c-}|, \\ I_{c+}/|I_{c-}|, & \text{if } I_{c+} > |I_{c-}|. \end{cases} \quad (1)$$

Intuitively it is clear that the larger the asymmetry \mathcal{A} is, the better the ratchet performs. A quantitative analysis [9, 23] showed that a large asymmetry allows one to achieve a wide operation range of drive current amplitudes (also known as rectification window), a large counter current (corresponding to a heavy load), against which rectification is still possible, and a large thermodynamic efficiency (ratio of output dc to input ac power). Thus, to fabricate a practically relevant ratchet one should design a system with high (critical current) asymmetry. An ideal ratchet has infinite asymmetry, *e.g.*, $I_{c+} = 0$ (or below the noise level), while $|I_{c-}|$ is finite and well above the noise level, or vice versa. To a first approximation, we aim for $\mathcal{A} \sim 10$. To our knowledge, such JRs were not reported until now with one notable exception [24]. In addition, previously demonstrated JRs were rather large, see Tab. I, which hampers their integration into micro- or nanoelectronic superconducting circuits.

^{*} C.S. and A.J. contributed equally to this work.

[†] gold@uni-tuebingen.de

In terms of their potential future use as nano-rectifiers of fluctuations (noise) and also for connecting many ratchets in series to obtain larger rectified voltages, one would like to down-size a single ratchet to sub- μm dimensions. In addition one would like to have the possibility to operate the JR over a wide range of temperatures T . Obviously, an upper limit in operation temperature is given by the transition temperature T_c of the superconducting material used for fabricating the JRs.

Recently, a new wave of interest emerged in the field of asymmetric (non-reciprocal) superconducting systems, termed “superconducting diodes” [25, 26] or “Josephson diodes” [27–33]. However, this term was already mentioned in 1997 in the context of the analysis of fluxon motion in long JJs with a step-like critical current density profile [34]. The superconducting diode is defined as a device with asymmetric critical currents I_{c+} and I_{c-} in positive and negative directions. In fact, these diodes are nothing else than the ratchets mentioned above. One can also use them as switches, *e.g.*, in digital (logic) circuits or as detectors or mixers, similar to a broad range of applications of semiconducting diodes. Below we will use the word diode to denote a universal device, while the word ratchet will be used as a diode with particular application for rectification of noise or ac signals. The first advantages of some of the diodes proposed recently is that those are based on specially engineered superconducting materials [25–27] and, therefore, can be structured down to the nanoscale, *e.g.*, down to 50...100 nm. Another advantage is that some of them [26–28] exhibit an asymmetry even at zero magnetic field. However, the values of asymmetry that were demonstrated up to now are mostly low. In Tab. I we compare the figures of merit for Josephson diodes. The critical temperature T_c of the materials used is often below 4 K (with one notable exception [32]), which prohibits operation even in liquid He at $T = 4.2$ K.

The aims of this work are: (I) to construct a highly asymmetric Josephson diode with a large critical current asymmetry, say, $\mathcal{A} \sim 10$; (II) reduce the essential area of the device to about $1 \mu\text{m}^2$ and (III) implement it using the high- T_c cuprate superconductor $\text{YBa}_2\text{Cu}_3\text{O}_7$ (YBCO), with $T_c \approx 90$ K that can operate in a wide temperature range (in our case up to 42 K).

To implement JJs with I_c asymmetry, we use junctions of in-line geometry, as described in the Ref. 35, however in the kinetic inductance limit. Such JJs in an external magnetic field B have a skewed point-symmetric $I_c(B)$ dependence. Thus, there are field values where the critical currents in the positive and negative directions are very different, see Appendix B for theoretical background.

II. FABRICATION

The fabrication of the ratchet devices starts on a $10 \times 10 \text{ mm}^2$ chip, purchased from CERACO GMBH. The chip consists of a 1-mm-thick (001)-oriented

$(\text{LaAlO}_3)_3(\text{Sr}_2\text{AlTaO}_6)_7$ (LSAT) substrate onto which a 20-nm-thick CeO_2 buffer layer followed by a YBCO film with thickness $d = 30$ nm was epitaxially grown by reactive coevaporation [36]. Subsequently a 20-nm-thick Au layer was deposited for electrical contacting. Micropatterning was done within two lithography steps. First, we utilize the MLA100 from HEIDELBERG INSTRUMENTS to pattern 200- μm -long microbridges with width $W \approx 4 \mu\text{m}$ (connected to larger contact pads for wire bonding) in the maP-1205 photoresist from MICRO RESIST TECHNOLOGY. Using Ar ion beam milling, we etch through all the thin film layers down to the substrate. Second, we remove the Au layer from the microbridges by means of a wet-etching process using TechniEtch ACI2 from MICROCHEMICALS.

To define the JJs and the circuit geometry we utilized the focused He ion beam (He-FIB) in a ZEISS Orion NanoFab He ion microscope (HIM) with 30 keV He^+ ions. By writing a line across a YBCO bridge with a moderate irradiation dose $D \sim 500 \dots 700$ ions/nm, the He-FIB irradiation creates a Josephson barrier [37–40], such that the corresponding JJ exhibits [39] an resistively-shunted junction (RSJ)-like I - V characteristic (IVC) with a Stewart-McCumber parameter $\beta_C \sim 1$. The critical current density j_c of such JJs decreases exponentially with increasing dose [39] D , and typically $I_c(T)$ vanishes with increasing T at $T \approx 40$ K for JJs irradiated with moderate dose [37, 38]. Instead, by writing a line with a high dose $D \sim 2000$ ions/nm, one creates a resistive wall (a barrier without supercurrent), which behaves similar to a semiconductor, *i.e.*, its resistance diverges as $T \rightarrow 0$, reaching a few $\text{M}\Omega$ or above at our main working temperature of 4.2 K [39]. Transmission electron microscopy analysis shows that on the atomic scale the resistive wall corresponds to damaged (amorphized) YBCO along the irradiated line [39] and mechanically stressed crystalline YBCO in the 50...100 nm vicinity of the amorphized region. [41] Further we use the term amorphous resistive wall (ARW) to remind the reader about both structural and electrical properties.

Before fabricating diodes within any of the prepatterned microbridges of width W , we wrote He-FIB lines with different moderate D values across several microbridges to produce a series of 4- μm -wide test JJs for calibration of the $j_c(D)$ dependence on the chip.

The JJ ratchets were then created in one He-FIB nanofabrication step to produce JJ barriers and ARWs in the inline JJ design, which is described in the next section. The dose for writing the JJ barriers was chosen to obtain the target j_c values (see below). The ARWs were always written with $D = 2000$ ions/nm.

III. DESIGN

One possibility to realize a highly asymmetric ratchet is to use a JJ with an in-line geometry as indicated in the HIM image in Fig. 1. The ARWs compel the bias current flow as indicated by the thick arrows, *i.e.*, the bias

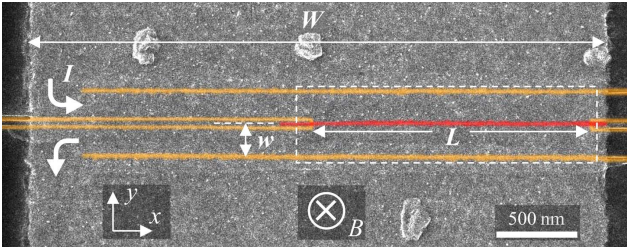


FIG. 1. Secondary electron HIM image of a reference microbridge (#A15) of the same geometry as device #A22 discussed in Sec. IV. For better visibility, #A15 has been irradiated with a high-dose He-FIB producing an ARW also at the place of the Josephson barrier. The He-FIB lines are colored to indicate where the device #A22 has ARWs (golden) written by high-dose He-FIB and the Josephson barrier (red) written by moderate-dose He-FIB. The thick arrows show the direction of bias current flow. The width of the whole YBCO bridge is W , the JJ length is L , and the electrode width (the distance between the JJ barrier and the upper and lower ARWs) is w . The dashed (white) rectangle shows the essential area A_e of the diode.

current I is injected and extracted from the (left) side, flows parallel to the JJ barrier of length L and across it. The spacing between the barrier and the ARWs is denoted as the electrode width w . Usually, for such an in-line geometry one observes a significant self-field effect (non-uniform magnetic field caused by and proportional to the bias current). This results in a skewed dependence of the critical current I_c on the magnetic field B (applied perpendicular to the thin film plane)[35]. In fact, for our very thin YBCO film with thickness $d \ll \lambda_L$ (typically $\lambda_L \approx 250$ nm for YBCO films), the kinetic inductance dominates. Therefore, it is more correct to speak about a phase gradient (of the macroscopic wavefunctions in the superconducting electrodes) along the barrier (instead of magnetic field) caused by the in-line bias configuration. Similar designs were proposed[42] as diodes very recently and already used for Nb|CuNi|Nb JJs[43] and YBCO grain-boundary JJs [44, 45], but for different purposes.

The planar thin-film JJs used in this work (even in the simplest geometry when the JJ crosses the whole bridge) are non-local [46]. Our geometry, see Fig. 1, is even more complicated than the one from Ref. 46.

A theoretical treatment of the $I_c(B)$ dependence for our JJ geometry has not been developed so far. Therefore, the estimations of target parameters for our JJ ratchets are possible only approximately, in the framework of the usual local model, see Appendix B. There we find that the key parameter that defines the asymmetry of the $I_{c\pm}(B)$ curves is the so-called *in-line geometry parameter*

$$f_I = \frac{1}{4\pi} \left(\frac{L}{\lambda_J} \right)^2, \quad (2)$$

see Appendix A for an estimation of λ_J . There it is shown that

$$\lambda_J^2 \propto \frac{w}{j_c \lambda_L^2}, \quad (3)$$

Further, having f_I we can calculate the (skewed) dependences of the normalized critical current $i_{c\pm} = I_{c\pm}/I_{c0}$ ($I_{c0} \equiv j_c L d$) on the applied normalized magnetic flux $f = \Phi/\Phi_0$ ($\Phi_0 \approx 2.068 \cdot 10^{-15}$ Wb is the magnetic flux quantum) for different values of f_I . We find that with increasing f_I the maximum asymmetry \mathcal{A}_{\max} (\mathcal{A} at an optimum value f_{opt} of f) increases rapidly and diverges for $f_I \geq f_I^* = \pi/4$. This happens because the smaller critical current $\min(|I_{c\pm}(B)|)$ vanishes. Experimentally, this divergence is suppressed since there is always a finite background I_c value. Accordingly, we estimate practically achievable values for $\mathcal{A}_{\max} \sim 10$. For details, see Appendix B.

Guided by predictions of the local model, we chose the target parameters, such as D (*i.e.*, j_c), L and w , to achieve the desired asymmetry and reasonable critical current.

The JJ physical length L was chosen to have the in-line geometry parameter $f_I \approx \pi/4$, *i.e.*, $L \approx \pi \lambda_J$ to achieve maximum possible asymmetry $\mathcal{A} \sim 10$ at the optimum flux bias point f_{opt} , see Appendix B. In this way JJ also remains in the short JJ limit. Since one of our goals is to make the size of the device as small as possible, we would like to have L as small as possible, *i.e.*, as small as possible λ_J .

The width w between the ARWs and JJ barrier should be chosen as small as possible to reduce λ_J and, accordingly, to reduce the size ($L \times w$) of the diode. However, w is limited by the mechanical damage around the ARWs.

Finally, the dose D was chosen to obtain j_c values that provide JJs with RSJ-like IVC[39] at $B = 0$ and to have a reasonable maximum critical current $I_{c0} = j_c d L$ in the range $5 \dots 30 \mu\text{A}$ at $T = 4.2$ K. Such values of I_{c0} are easily measurable and later allow one to investigate not only the limit of small thermal fluctuations $k_B T/E_J(T) \ll 1$, but also the limit of large thermal fluctuations in a reasonably broad temperature range within our target temperature range of 4.2–42 K. Here $E_J(T) = \Phi_0 I_{c0}(T)/(2\pi)$ is the temperature-dependent Josephson energy. We note that $j_c(T)$ affects λ_J .

At the end we have fabricated and tested a set of several diodes with the parameters distributed around the target parameters of the local model.

IV. EXPERIMENTAL RESULTS

Here we present experimental data only for the device #A22 with $L = 1750$ nm and $w = 200$ nm. The barrier was written with $D = 530$ ions/nm, which resulted in a maximum $I_{c0} \approx 14 \mu\text{A}$ at $T = 4.2$ K (see below). Thus, $j_c \approx 27$ kA/cm² and $\lambda_J \approx 1.25 \mu\text{m}$ at 4.2 K, see Appendix A for details.

References	Type	\mathcal{A}	\bar{V} (μV)	\bar{P}_{out} (nW)	η (%)	A_e (μm^2)	T_{op} (K)
Carapella (2001)[16]	ALJJ	1.2	5	-	-	44500	6.5
Beck (2005)[8]	ALJJ	2.2	20	-	-	5700	6
Sterck (2005,2009)[14, 15]	3JJ SQUID	2.5	25	-	-	1125	4.2
Wang (2009)[17]	ALJJ	2.8	100	-	-	800	4.2
Knufinke (2012)[9, 47]	ALJJ E3	1.6	40	16 [‡]	25[48]	4900	4.2
Menditto (2016)[22]	φ junction	2.5	150	-	-	2000	1.7
Golod (2022)[24, 49]	in-line JJ	4	8	-	70[48]	7.2	7
Wu (2022)[27]	NbSe ₂ Nb ₃ Br ₈ NbSe ₂	1.07	800[50]	-	3.4[48]	3.7	0.02
Jeon (2022)[28]	Nb Pt+YIG Nb	2.07	-	-	35[48]	4	2
Pal (2022)[29]	Nb Ti NiTe ₂ Ti Nb	2.3	8[50]	-	40[48]	~ 3	3.8
Baumgartner (2022)[30]	Al 2DEG Al	2	-	-	30[48]	7	0.1
Paolucci (2023) [31]	2JJ SQUID	3	8	-	6[48]	72	0.4
Gosh (2024) [32, 33]	twisted BSCCO flakes	4	25[50]	-	60[48]	100	80
This work	in-line JJ	7	212	0.2	74	1.0	4.2–42

TABLE I. Comparison of key parameters of Josephson diodes from literature. \mathcal{A} is the asymmetry (1), \bar{V} is the maximum rectified voltage (for optimum drive amplitude I_{ac}), \bar{P}_{out} is the maximum output power measured, η is the maximum thermodynamic efficiency reached. A_e is defined as the area of the part of the device essential for its operation, excluding electrodes, parts that can be safely “cut off” without affecting the operation. If devices should be combined into an array, A_e is the area of one period of such an array. For many cited works we estimated A_e from the size of the minimum rectangle containing the part of the device essential for its operation.

A. Characterization

The electric transport measurements are done in a 4-point configuration and were performed in liquid He at $T = 4.2\text{K}$. The IVC of the device #A22 at $B = 0$ is shown in Fig. 2(a). The IVC is RSJ-like with symmetric critical currents and without hysteresis. To find the optimal working point of the ratchet, we measure the dependence $I_c(B)$. The field is applied perpendicular to the sample plane by means of a coil. The $I_c(B)$ dependence is shown in Fig. 2(b). The optimum working point corresponds to the maximum of \mathcal{A} , see definition (1). Using the data from Fig. 2(b) we display $\mathcal{A}(B)$ on the same plot to determine the value of B_{opt} , where $\mathcal{A}(B)$ has its maximum ≈ 7 . Figure 2(a) also shows the IVC of the ratchet at $B = B_{\text{opt}}$. The critical currents are rather asymmetric.

B. Quasistatic deterministic drive

For demonstration of the ratchet operation in a quasistatic deterministic regime we apply $B = B_{\text{opt}}$ to induce maximum \mathcal{A} and drive the ratchet with a sinusoidal current

$$I(t) = I_{\text{ac}} \sin(2\pi ft), \quad (4)$$

where we typically use $f = 200\text{Hz}$, i.e., we operate in the adiabatic regime $f \ll f_c$ [13, 14, 51], with the characteristic frequency $f_c = I_c R / \Phi_0 \sim 300\text{GHz}$ ($R \approx 50\Omega$ is the JJ normal resistance). The $I(t)$ waveform is generated by a programmable DAC card with an update rate of 10 kHz (samples/sec). For a given continuously applied waveform with amplitude I_{ac} we measure the voltage \bar{V} averaged over one period of the drive $T = 1/f = 5\text{ms}$,

i.e.,

$$\bar{V} = \frac{1}{T} \int_0^T V(t) dt. \quad (5)$$

Technically this is done by collecting 500 voltage samples with a sampling rate of 100 kHz (interval between the samples $10\mu\text{s}$) by the programmable ADC card. By repeating the measurement of \bar{V} for different values of I_{ac} we obtain the *rectification curve* $\bar{V}(I_{\text{ac}})$ shown in Fig. 3(a) as the red curve, labeled with “idle”, which means that the drive is a pure ac drive without any dc counter current, i.e., $I_{\text{dc}} = 0$. One can see that for very low amplitudes $I_{\text{ac}} \lesssim I_{c+}$ the rectification is absent as the ac bias point never reaches the voltage branches of the IVC during ac-driving. For $I_{c+} \lesssim I_{\text{ac}} \lesssim |I_{c-}|$ the bias point reaches only the positive voltage branch of the IVCs during the positive semi-period, which results in a finite \bar{V} that grows with I_{ac} , until $\bar{V}(I_{\text{ac}})$ reaches its maximum value \bar{V}_{max} at $I_{\text{ac,max}} \approx |I_{c-}|$. Finally, at $I_{\text{ac}} \approx I_{c-}$ the bias point also reaches the negative voltage branch of the IVC during the negative semi-period and the average voltage drops with further increasing I_{ac} and asymptotically approaches zero for $I_{\text{ac}} \gg |I_{c-}|$. [52]

The rectification is *efficient roughly* for I_{ac} between I_{c+} and I_{c-} . [53] If one wants to construct a ratchet which rectifies a large range of input amplitudes, one should ideally have $I_{c+} \ll |I_{c-}|$ (or $|I_{c-}| \ll I_{c+}$), i.e., large \mathcal{A} . We observe a maximum rectified voltage $\bar{V} \approx 212\mu\text{V}$, which is one of the best among similar devices, see Tab. I.

Up to now our ratchet is idle, i.e., it does not produce any useful work (output power). In terms of a particle in an asymmetric periodic potential, this means that the particle is driven by a pure ac drive to the right (easy direction), but stays roughly at the same energy/height. To produce work one has to load the ratchet. One pos-

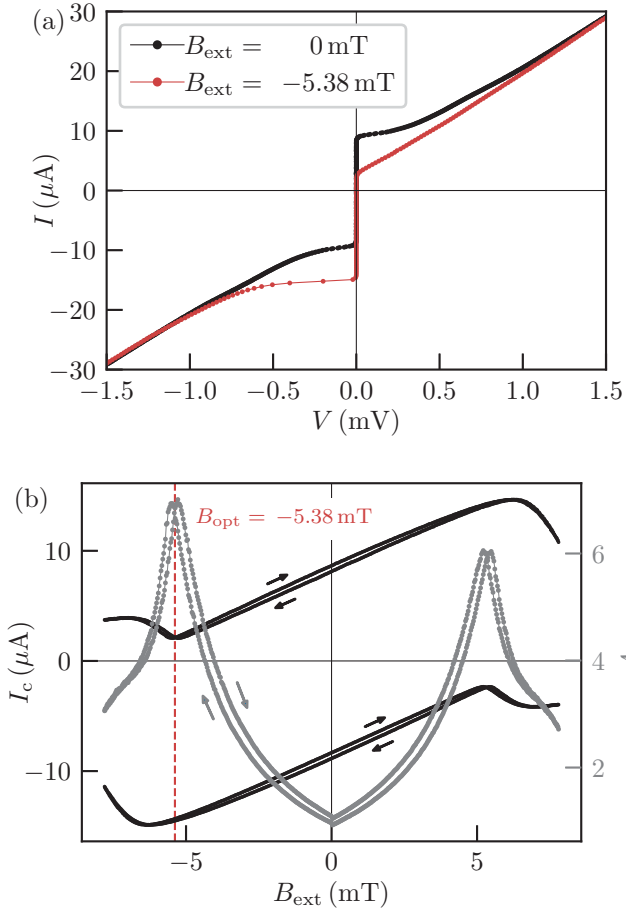


FIG. 2. Electric transport data for sample #A22: (a) IVCs measured in both bias-current sweep-directions at $B = 0$ (black) and at optimal applied field B_{opt} (red). $I_{c+}(0) \approx |I_{c-}(0)| \approx 10 \mu\text{A}$, while $I_{c+}(B_{\text{opt}}) \approx 2.0 \mu\text{A}$ and $|I_{c-}(B_{\text{opt}})| \approx 14.2 \mu\text{A}$ (taken from IVCs with a voltage criterion of $1 \mu\text{V}$), which results in $\mathcal{A}(B_{\text{opt}}) \approx 7$. Both IVCs are somewhat rounded around the critical currents due to thermal fluctuations and nonuniformities of the JJ, so $I_{c\pm}$ could be determined experimentally only approximately. (b) $I_{c\pm}(B)$ measured in both B sweep directions (black) and $\mathcal{A}(B)$ (grey) numerically calculated from the $I_{c\pm}(B)$ data. The optimum field $B_{\text{opt}} \approx -5.38 \text{ mT}$.

sibility [9] is to tilt the potential in such a way that the ratchet effect will transport the particle uphill. In this case one can also address the question “how strong is the ratchet”, *i.e.*, against which counter tilt the ratchet can still transport the particle. Experimentally, it is rather easy to tilt the potential just by applying an additional dc bias counter current to the JJ. If our rectified voltage $\bar{V} > 0$ then one needs a counter current $I_{\text{dc}} < 0$. Then, the total applied current is

$$I(t) = I_{\text{ac}} \sin(2\pi ft) + I_{\text{dc}}. \quad (6)$$

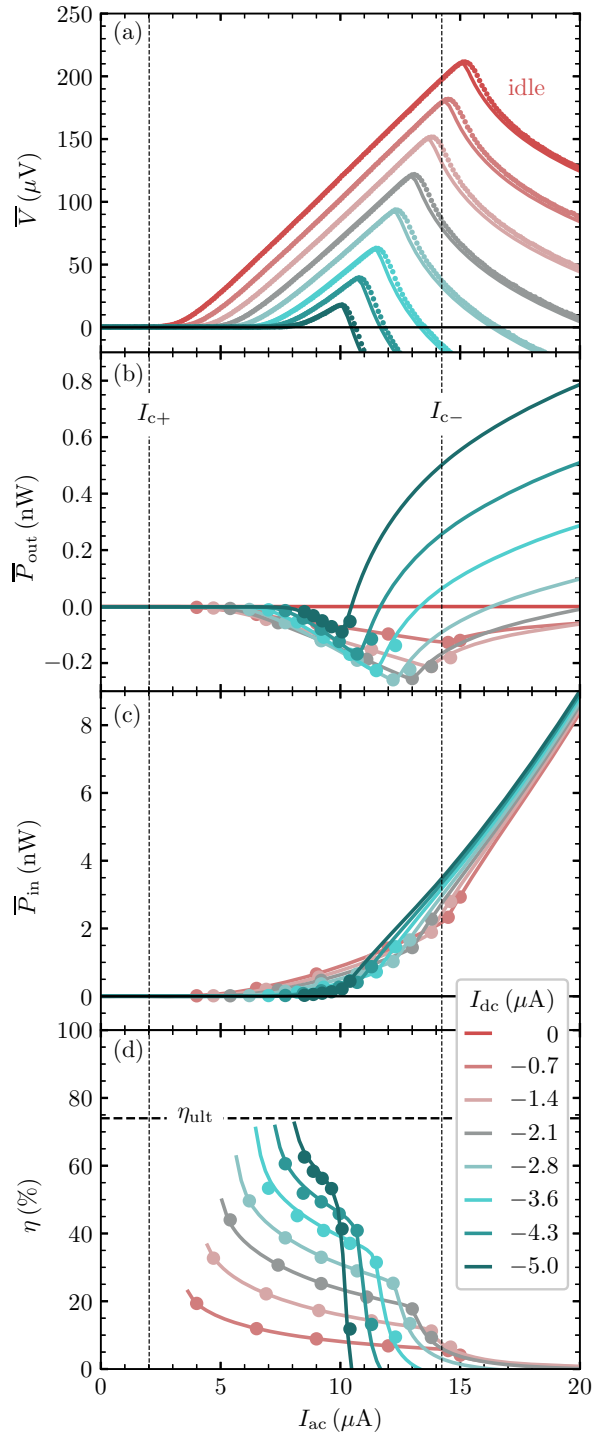


FIG. 3. Performance of JR (sample #A22) vs. ac drive amplitude I_{ac} ($f = 200 \text{ Hz}$) at $B = B_{\text{opt}}$, for different values of counter current $I_{\text{dc}} \leq 0$. (a) rectification curves $\bar{V}(I_{\text{ac}})$, (b) output power $P_{\text{out}}(I_{\text{ac}})$, (c) input power $P_{\text{in}}(I_{\text{ac}})$ and (d) efficiency $\eta(I_{\text{ac}})$. Symbols show experimental data. Lines are calculated from the high-resolution experimental IVC as described in the text.

The rectification curves

$$\bar{V}(I_{ac}) = \frac{1}{T} \int_0^T V(I(t)) dt. \quad (7)$$

for several I_{dc} values are shown in Fig. 3(a). One can see that transport against the counter current still takes place i.e., $\bar{V} > 0$, although the average voltage (particle speed) and accordingly, the maximum average voltage \bar{V}_{max} , decreases with increasing I_{dc} . The rectification range shrinks with increasing $|I_{dc}|$, and for large I_{ac} the transport reverses ($\bar{V} < 0$). The stopping current, i.e., the (minimum) counter current, for which the ratchet does not transport anymore in the easy direction for any I_{ac} , is theoretically given by [9] $I_{stop} = (I_{c+} - |I_{c-}|)/2 \approx -6.1 \mu\text{A}$, which agrees quite well with the data presented in Fig. 3(a). Note that the ratchet loaded with $I_{dc} < 0$ produces negative \bar{V} at large I_{ac} . This motion in the difficult direction is simply caused by the applied I_{dc} , which overweights the ratchet effect.

Since the ratchet with $I_{dc} < 0$ transports the particle uphill, it produces an (average) output power

$$\bar{P}_{out} = \frac{1}{T} \int_0^T V(I(t)) \cdot I_{dc} dt = \bar{V} \cdot I_{dc}. \quad (8)$$

Thus, to obtain plots $\bar{P}_{out}(I_{ac})$ one should just multiply each $\bar{V}(I_{ac})$ curve from Fig. 3(a) by the corresponding value of I_{dc} . The result is shown in Fig. 3(b). Note that since $I_{dc} \leq 0$, we formally get $\bar{P}_{out} \leq 0$ (if $\bar{V} > 0$), which means that we generate power rather than consume it. Obviously, the idle ratchet ($I_{dc} = 0$) produces $\bar{P}_{out}(I_{ac}) \equiv 0$. Then by increasing the counter current $|I_{dc}|$ the amplitude of $\bar{P}_{out}(I_{ac})$ curves first grows and then decreases in accordance with the product in Eq. (8), where the amplitude of $\bar{V}(I_{ac})$ decreases with $|I_{dc}|$ down to zero at I_{stop} , at which $\bar{V}(I_{ac})$ and $P_{out}(I_{ac})$ change sign. Note that in the parts of the curves, where $P_{out} > 0$ (corresponding to parts with $\bar{V} < 0$ in Fig. 3(a)), the ratchet consumes the power from dc counter current source. Thus, the maximum output power in the regime $P_{out} < 0$ is expected for an intermediate load between 0 and I_{stop} .

Similarly, the input power is given by

$$\bar{P}_{in} = \frac{1}{T} \int_0^T V(I(t)) \cdot I_{ac} \sin(2\pi ft) dt. \quad (9)$$

Equation (9) cannot be simplified in a similar way as Eq. (8). Therefore, to determine \bar{P}_{in} , one needs simultaneously measured $I_{ac} \sin(2\pi ft)$ and $V(t)$ profiles. Those were measured for six different values of I_{ac} for each I_{dc} value. The results are presented in Fig. 3(c) by symbols. Roughly, one notes three regions on the plots. For low I_{ac} the power vanishes as the ratchet never enters the voltage state. For intermediate values of I_{ac} (branches with slight slope in Fig. 3(c)) the ratchet dissipates only at the positive voltage branch during some part of the positive semi-period of the drive and, finally, for large

I_{ac} (branches with strong slope in Fig. 3(c)) the ratchet dissipates even more during both positive and negative semi-periods.

In the quasi-static regime of operation, all information on the ratchet performance and its figures of merit are contained in the IVCs. Therefore, having a (high resolution) experimental $V(I)$ (as a list of numerical I and V values), one can calculate all characteristics like $\bar{V}(I_{ac})$, \bar{P}_{in} , \bar{P}_{out} , etc. for different values of the load I_{dc} numerically, by ‘‘applying’’ the current $I(t)$ given by Eq. (6) to the IVC and calculating the integrals (7)–(9) numerically. In this way one can produce quite many points per curve (esp. relevant for \bar{P}_{in}). The results are also presented in Fig. 3 as solid lines and show only a minor difference with those measured experimentally.

Finally, having \bar{P}_{out} and \bar{P}_{in} one can calculate the *thermodynamic efficiency*

$$\eta(I_{ac}) \equiv -\frac{\bar{P}_{out}(I_{ac})}{\bar{P}_{in}(I_{ac})}. \quad (10)$$

Note that *thermodynamic efficiency* η should not be confused with the ‘‘efficiency’’ given by

$$\eta_{ult} = \left| \frac{|I_{c-}| - |I_{c+}|}{|I_{c-}| + |I_{c+}|} \right| \equiv \frac{\mathcal{A} - 1}{\mathcal{A} + 1}, \quad (11)$$

used in many publications. On the one hand, η_{ult} just characterizes the degree of asymmetry of critical currents and can be expressed via \mathcal{A} used in this work. On the other hand, η_{ult} represents the maximum possible (ultimate [9, 23]) thermodynamic efficiency that can be reached for a given asymmetry theoretically.

A set of $\eta(I_{ac})$ curves for different load values are shown in Fig. 3(d). Each $\eta(I_{ac})$ curve has a sharp maximum just in the beginning of the rectification window, as predicted by the model [9, 23]. As a function of I_{dc} the $\eta(I_{ac})$ curves reach their maximum amplitude for large counter current $|I_{dc}|$ close to I_{stop} , where the rectification window is tiny. In this regime the value of η approaches its theoretical value η_{ult} ($\approx 75\%$ for #A22).

We note that the efficiency is cut (not calculated) for $I_{ac} < I_{c+}$. In this range, both $\bar{P}_{out} \rightarrow 0$ and $\bar{P}_{in} \rightarrow 0$ (theoretically) so that η has a very large uncertainty. In fact, any measurement (fluctuation) or numerical error in \bar{P}_{in} will result in a huge fluctuation of η . In other words, η will have error bars much larger than the value of η itself. Therefore, the calculation of η was not performed, if \bar{P}_{in} was smaller than a certain limit (typically 5 pW). This is a common problem for the evaluation of the performance of any ratchet operated with small drive amplitudes.

C. Quasistatic stochastic drive

In this section, starting from the experimentally measured asymmetric IVC, we numerically calculate rectification of a random driving force $I(t) = \Xi(t)$ with a

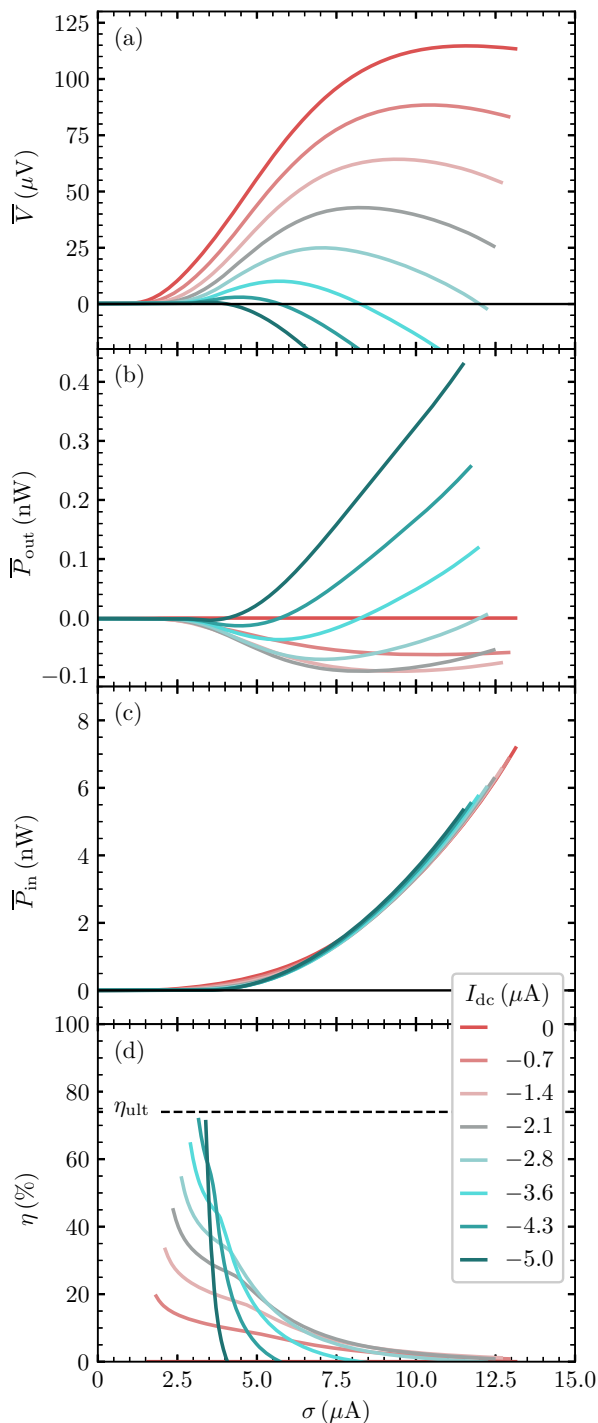


FIG. 4. Performance of JR (calculated from the IVC at $B = B_{\text{opt}}$ of sample #A22) vs distribution width (noise amplitude) σ of a quasistatic stochastic drive current, for different values of counter current $I_{\text{dc}} \leq 0$. (a) Rectification curves $\bar{V}(\sigma)$, (b) $\bar{P}_{\text{in}}(\sigma)$ and (c) $\bar{P}_{\text{out}}(\sigma)$ and (d) $\eta(\sigma)$. For the calculations we used a 3σ cutoff during integration, see Eq. (14) and the following text.

Gaussian distribution of the probability density

$$G(I, \sigma) = \frac{1}{\sqrt{2\pi}\sigma} \exp\left(-\frac{I^2}{2\sigma^2}\right). \quad (12)$$

Here the distribution width σ plays a role of the amplitude of the noise. In fact, if one has a realization of a random process $\Xi(t)$ with amplitude 1 (dimensionless), the process $\sigma \cdot \Xi(t)$ has the distribution width σ . We will consider *quasistatic* noise, *i.e.*, each random current value $\sigma \cdot \Xi(t_i)$ is applied and kept long enough to measure the voltage $V(\sigma \cdot \Xi(t_i))$ (IVC), then the next random current value $\sigma \cdot \Xi(t_{i+1})$ is applied and so on. In other words, the bandwidth of this noise is much smaller than the typical Josephson frequencies (so that the concept of IVC makes sense) and our measurement setup bandwidth. Then the average voltage V_{dc} (to distinguish it from the voltage \bar{V} averaged over one period in the case of a deterministic periodic drive) is calculated. Due to quasi-staticity, the result can be again obtained just from the experimentally measured IVC numerically as

$$\begin{aligned} V_{\text{dc}}(\sigma) &= \lim_{T \rightarrow \infty} \frac{1}{T} \int_0^T V(\sigma \cdot \Xi(t) + I_{\text{dc}}) dt \\ &= \lim_{N \rightarrow \infty} \frac{1}{N} \sum_{i=1}^N V(\sigma \cdot \Xi(t_i) + I_{\text{dc}}). \end{aligned} \quad (13)$$

Numerically, the expression (13) needs a long integration time to converge. However, for ergodic random processes this can be drastically simplified to a convolution of the Gaussian random distribution with the IVC:

$$V_{\text{dc}}(\sigma) = \int_{-\infty}^{+\infty} G(I, \sigma) V(I + I_{\text{dc}}) dI. \quad (14)$$

Note that the experimental $V(I)$ is available (measured) only in certain limited current range. Therefore, to perform the integration in Eq. (14) in practice we integrate from -3σ to $+3\sigma$, thus, cutting off the tails of the Gaussian distribution.

A set of rectification curves $V_{\text{dc}}(\sigma)$ for different counter currents I_{dc} are shown in Fig. 4(a). Qualitatively the curves look very similar to the $\bar{V}(I_{\text{ac}})$ curves for a deterministic sinusoidal ac drive. However, the maximum rectified voltage (in the idle regime) became almost twice smaller. The curves are also much more smooth, which is understandable considering the Gaussian distribution of the noise. However, the stopping force does not change, which is easy to understand from the IVC. Namely, the applied counter current I_{dc} basically shifts the origin of the IVC so that the IVC becomes more symmetric. Roughly the rectification vanishes when the positive and negative critical currents become equal, *i.e.*, $I_{c+} - I_{\text{dc}} \approx |-I_{c-} + I_{\text{dc}}|$ regardless what kind of drive is applied.

Furthermore, a set of $\bar{P}_{\text{in}}(\sigma)$, $\bar{P}_{\text{out}}(\sigma)$ and $\eta(\sigma)$ curves for different values of I_{dc} are shown in Fig. 4(b)–(d). One can see that here the curves are also similar to the ones

with a sinusoidal drive. In particular, the efficiency $\eta(\sigma)$ for strong load (counter current) still tends to almost reach the ultimate efficiency η_{ult} .

We would like to point out that rectification of the quasistatic Gaussian noise does not contradict the second law of thermodynamics. In fact, equilibrium thermal fluctuations produce a noise current with a Gaussian probability density and amplitude

$$\sigma = \sqrt{\frac{2k_B T \cdot \Delta f}{R}}, \quad (15)$$

where Δf is the bandwidth of the system (width of the white noise spectrum). Quasistatic noise essentially means that $\Delta f \ll f_{\text{setup}} \ll f_J$. For example, for $\Delta f = 10$ kHz according to Eq. (15) the amplitude of the thermal noise is $\sigma \sim 0.15$ nA, while we apply the amplitudes at least 10^4 times larger, see Fig. 4. This essentially means that our noise is not thermal.

V. CONCLUSIONS

We demonstrated the design, fabrication and quasistatic operation of a Josephson diode “drawn” into a YBCO thin-film micro-bridge using He-FIB. The ratchet shows record figures of merit, see Tab. I, and its direction of rectification depends on the sign of the applied (optimum) field. In particular, the ratchet occupies an *essential* area $\approx 1 \mu\text{m}^2$, which is the smallest in Tab. I. At the optimum magnetic field the ratchet shows an impressive asymmetry $\mathcal{A} \approx 7$, close to the similar design based on Nb[24, 43]. As a consequence, it demonstrates a maximum rectified voltage $\bar{V} \approx 212 \mu\text{V}$ for a sine-drive and a $\bar{V} \approx 115 \mu\text{V}$ (calculated from experimental IVC) for a random Gaussian drive. In both cases the ratchet shows a large stopping force (in accordance with the value of \mathcal{A} , see Refs. 9 and 23), and the thermodynamic efficiency approaching the theoretical limit (ultimate efficiency) in certain regimes. However, there is a general trade-off between maximum output power and maximum efficiency that occur at different values of parameters (drive amplitude and counter force). The only ratchet in Tab. I that shows larger output power (estimated) is the one reported in Ref. 9. There, the ratchet design was a large ALJJ with very high I_c .

Preliminary measurements show that the ratchets discussed in the present paper operate at temperatures up to ~ 40 K, where the critical currents of JJ tend to zero, while the thermal energy increases by one order of magnitude. Detailed results for the noise-driven ratchet will be published elsewhere.

ACKNOWLEDGMENTS

This work was funded by the Deutsche Forschungsgemeinschaft (DFG) via projects No. GO-1106/6 and KL-

930/17. A. J. thanks his father for financial support during his study. We thank M. Turad and R. Löffler for invaluable help with “Orion Nanofab”.

Appendix A: Estimating λ_J

To estimate λ_J we use the usual expression [35]

$$\lambda_J = \sqrt{\frac{\Phi_0}{2\pi \cdot \ell_J \cdot j_c}}, \quad (A1)$$

rewritten explicitly isolating ℓ_J — an inductance per JJ length times thickness d of the superconducting electrodes forming the JJ when the current flows along the Josephson barrier (units are $\text{H} = \text{V} \cdot \text{s}/\text{A}$, like for inductance). [54] Thus, in our planar case, the total inductance of the two pieces of superconducting films on both sides of the barrier is given by $L_\Sigma = \ell_J \cdot L/d$.

In our particular case $\ell_J = 2\ell$, where ℓ corresponds to one superconducting electrode. The JJ barrier thickness (created by He-FIB) is considered to be negligible in comparison with the electrode width w . The total inductance L_{el} of a piece of superconducting electrode of length L and (film) thickness d is given by $L_{\text{el}} = \ell \cdot L/d$, i.e., $L_\Sigma = 2L_{\text{el}}$

In our ultra-thin-film limit ($d = 30$ nm, while the London penetration depth $\lambda_L \approx 250$ nm) we can safely assume that the inductance is purely kinetic. So when the current flows in the superconducting film along the barrier of the JJ, the associated kinetic energy is given by

$$E_k = n_s \frac{m v_s^2}{2} \cdot V', \quad (A2)$$

where $V' = Lwd$ is the volume of the film, while m , n_s and v_s are mass, concentration and average velocity of “superconducting” electrons, respectively.

Using the relation for the supercurrent density $j_s = n_s v_s e$, we can rewrite Eq. (A2) as

$$E_k = \frac{m j_s^2}{2 n_s e^2} \cdot Lwd = \frac{m I_s^2}{2 n_s e^2 w^2 d^2} \cdot Lwd = \frac{mL}{n_s e^2 w d} \frac{I_s^2}{2}, \quad (A3)$$

where we have introduced the supercurrent $I_s = j_s \cdot w \cdot d$, which assumes a homogenous j_s in our electrodes with $w \ll \lambda_{\text{eff}} = \lambda_L^2/d$. We remind that in the framework of the London theory

$$\lambda_L^2 = \frac{m}{\mu_0 n_s e^2}. \quad (A4)$$

Thus,

$$E_k = \mu_0 \lambda_L^2 \frac{L}{wd} \frac{I_s^2}{2}. \quad (A5)$$

The kinetic inductance is therefore

$$L_k = \mu_0 \lambda_L^2 \frac{L}{wd}, \quad (A6)$$

i.e.,

$$\ell = \mu_0 \lambda_L^2 \frac{1}{w}, \quad (\text{A7})$$

For our parameter $w = 200$ nm we get $\ell_J = 2\ell = 0.79$ pH. This, according to Eq. (A1) with $j_c = 27$ kA/cm², gives $\lambda_J \approx 1.2$ μ m.

Quantitatively, the inductance of the JJ barrier of length L (Josephson inductance at infinitesimal current, see Ref. 35) is given by

$$L_J = \frac{\Phi_0}{2\pi I_c} = \frac{\Phi_0}{2\pi j_c \cdot L \cdot d}. \quad (\text{A8})$$

Assuming that $L \rightarrow \infty$ ($L \gg \lambda_J$) λ_J is the characteristic length, across which the bias current injected from the edge distributes and tunnels through the JJ barrier. At this length the Josephson inductance of the λ_J -piece of the barrier is equal to the inductance of the λ_J -piece of both electrodes, *i.e.*,

$$L_J|_{L=\lambda_J} = 2 L_k|_{L=\lambda_J}.$$

Inserting, L_k and L_J from Eqs. (A6) and (A8), we obtain

$$\frac{\Phi_0}{2\pi j_c \cdot \lambda_J \cdot d} = 2\mu_0 \lambda_L^2 \frac{\lambda_J}{wd}$$

From here

$$\lambda_J^2 = \frac{\Phi_0 wd}{2\pi j_c d 2\mu_0 \lambda_L^2} = \frac{\Phi_0 w}{2\pi j_c 2\mu_0 \lambda_L^2} = \frac{\Phi_0}{2\pi j_c \ell_J},$$

i.e., exactly as given by Eq. (A1) with $\ell_J = 2\ell$ from Eq. (A7).

Appendix B: In-line geometry.

1. Derivation of $I_c(B)$

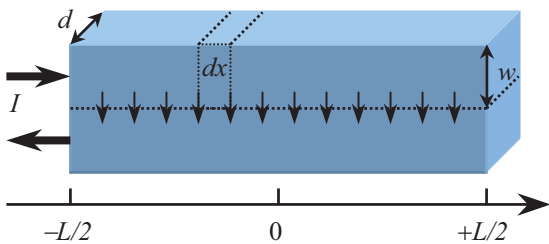


FIG. 5. The JJ of in-line geometry consisting of two superconducting films and a very thin barrier (dotted). The arrows indicate the current I injected/collected at the left edge and flowing through the barrier.

Following Ref. 35, we consider a JJ of inline geometry spanning along x from $-L/2 \dots +L/2$. The bias current I

is injected to and collected from the left side of the superconducting electrodes. We assume that the JJ is short, *i.e.*, $L \lesssim 4\lambda_J$, and, for now, we assume zero applied magnetic field. The bias current distributes along the whole JJ length L to tunnel through the barrier. Since the JJ is short, we assume that the Josephson phase $\phi(x)$ is almost constant across the barrier. In this case, the Josephson current density across the barrier $j_s(x)$ is constant too. Then, we write a current continuity (1st Kirchoff) equation at an arbitrary point x inside the JJ.

$$I_L(x + dx) - I_L(x) = j_s(x) \cdot dx \cdot d,$$

which, for $dx \rightarrow 0$ gives

$$\frac{\partial I_L(x)}{\partial x} \equiv I'_L(x) = j_s(x) \cdot d, \quad (\text{B1})$$

where $I_L(x)$ is the current flowing along the top superconducting electrode. Considering our inline biasing scheme the boundary conditions (BCs) for $I_L(x)$ are

$$I_L(-L/2) = I, \quad I_L(+L/2) = 0. \quad (\text{B2})$$

By solving Eq. (B1) with BCs (B2) we get an explicit expression for

$$I_L(x) = -j_s d [x - L/2] = -I \left[\frac{x}{L} - \frac{1}{2} \right], \quad (\text{B3})$$

where we have used the obvious fact that the whole bias current finally tunnels through the JJ, *i.e.*, $I = j_s d L$.

The current $I_L(x)$ flowing through the kinetic inductance dL_k of the dx piece of the top/bottom electrode creates a phase difference (of the macroscopic wavefunction of the electrode)

$$\theta(x + dx) - \theta(x) = \frac{2\pi}{\Phi_0} \cdot dL_k I_L(x) = \frac{2\pi}{\Phi_0} \cdot \mu_0 \lambda_L^2 \frac{dx}{wd} I_L(x),$$

which for $dx \rightarrow 0$ gives

$$\theta'(x) = \frac{2\pi}{\Phi_0} \cdot \mu_0 \lambda_L^2 \frac{I_L(x)}{wd}, \quad (\text{B4})$$

where $\mu_0 \lambda_L^2$ is the specific kinetic inductance, see Appendix A.

By substituting the expression (B3) into Eq. (B4) and solving it, we obtain

$$\theta(x) = \frac{2\pi}{\Phi_0} \cdot \frac{\mu_0 \lambda_L^2}{wd} I \left(\frac{x}{2} - \frac{x^2}{2L} \right). \quad (\text{B5})$$

For the moment we omitted the integration constant as it will be added later when we consider and maximize the supercurrent.

The Josephson phase $\phi(x)$ is the difference of the phases $\theta_1(x)$ and $\theta_2(x)$ in electrodes 1 and 2. Since the electrode currents $I_{L1}(x)$ and $I_{L2}(x)$ flow in opposite directions, with accuracy of a constant one can write $\theta_2(x) = -\theta_1(x)$. Therefore, $\phi(x) = 2\theta_1(x)$, see Eq. (B5).

Following Ref. 35, we ignore the parabolic bending of the Josephson phase and keep only the linear term (global behavior), *i.e.*,

$$\phi(x) \approx \frac{2\pi}{\Phi_0} \cdot \frac{\mu_0 \lambda_L^2}{wd} \cdot x \cdot I. \quad (\text{B6})$$

This dependence is very similar to the linear Josephson phase created by an applied magnetic field B perpendicular to the film plane

$$\phi'(x) = \frac{2\pi}{\Phi_0} d_{\text{eff}} B, \text{ or } \phi(x) = \frac{2\pi}{\Phi_0} d_{\text{eff}} B x = 2\pi f \frac{x}{L}, \quad (\text{B7})$$

where we have introduced the normalized flux $f \equiv \Phi/\Phi_0$, where $\Phi \equiv Bd_{\text{eff}}L$ is the total magnetic flux threading the JJ. In our geometry $d_{\text{eff}} = 2\lambda_L \tanh w/\lambda_L \approx 2w$. The linear Josephson phase in Eq. (B6) is proportional to the bias current I . In Ref. 35 this is called a self-field effect. In our case the effect is exactly the same, but due to kinetic nature of the electrode's inductance the magnetic field induced by the bias current I as such is not present.

To obtain the total supercurrent, but now also including an applied magnetic field, we have to add the phase gradients resulting from both bias current and applied field. The ansatz reads

$$\phi(x) = 2\pi(f + f_I \cdot i) \frac{x}{L} + \phi_0, \quad (\text{B8})$$

where $i = I/I_{c0}$ is the normalized bias current and

$$f_I \equiv \frac{\mu_0 \lambda_L^2 \frac{L}{wd} I_{c0}}{\Phi_0} = \frac{L_K I_{c0}}{\Phi_0} = \frac{\Phi_{I_{c0}}}{\Phi_0}, \quad (\text{B9})$$

characterizes the strength of the “self-field” effect (Josephson-phase gradient due to bias current). It is defined as pseudo-flux $\Phi_{I_{c0}}$ through the kinetic inductance $L_k = \mu_0 \lambda_L^2 \frac{L}{wd}$ of the whole top electrode when one sends a current I_{c0} through it.

Following the standard procedure to find the total supercurrent

$$I_s(f, i, \phi_0) = d \cdot \int_{-L/2}^{+L/2} j_c \sin \phi(x) dx$$

with $\phi(x)$ given by Eq. (B8) and then maximizing $I_s(f, i, \phi_0)$ with respect to ϕ_0 we get for the normalized critical current $i_c = I_c/I_{c0}$

$$i_c(f, i_c) = \pm \frac{\sin[\pi(f + f_I i_c)]}{\pi(f + f_I i_c)}, \quad (\text{B10})$$

where $I_{c0} \equiv j_c L d$ is the maximum possible critical current through the barrier at $f = f_I = 0$. Note, that by using the definition (A1) of λ_J , one can rewrite the expression for f_I in a very simple and understandable form, namely

$$f_I = \frac{1}{4\pi} \frac{L^2}{\lambda_J^2}. \quad (\text{B11})$$

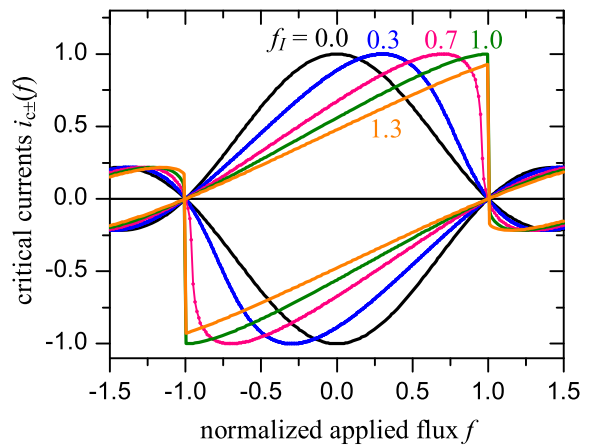


FIG. 6. A family of asymmetric $i_{c\pm}(f)$ curves for different f_I obtained by solving the eq. (B10) numerically.

2. Optimal parameters

The final $i_c(f)$ dependence is given by the implicit expression (B10). For fixed values of f_I and f we solved this equation numerically to obtain $i_{c\pm}(f)$ plots for several different values of f_I , see Fig. 6. With increasing f_I the $i_{c\pm}(f)$ plots depart from a symmetric Fraunhofer pattern ($f_I = 0$ curve) and become skewed, however they are still point-symmetric with respect to the origin. As f_I grows the two critical currents $i_{c+}(f)$ and $i_{c-}(f)$ become rather different for $|f|$ somewhat below 1 thus giving high asymmetry. At $f_I > f_I^* = \pi/4 \approx 0.785$ one of the $i_{c\pm}(f)$ curves develops a discontinuous jump at $f = \pm 1$ from high i_c (absolute) values to low ones.

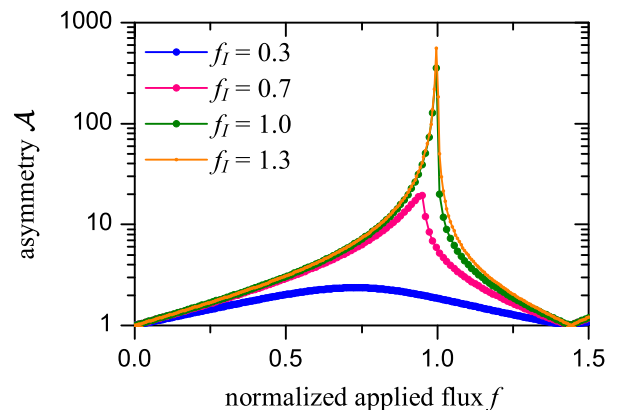


FIG. 7. Asymmetry parameter $\mathcal{A}(f)$ for different values of f_I obtained from the curves in Fig. 6 using the definition (1).

To be more specific, in Fig. 7 we have plotted the dependence of the asymmetry $\mathcal{A}(f)$ (only for positive f , negative f are similar) for different values of f_I . There is an optimum applied field f_{opt} , for which \mathcal{A} has a maxi-

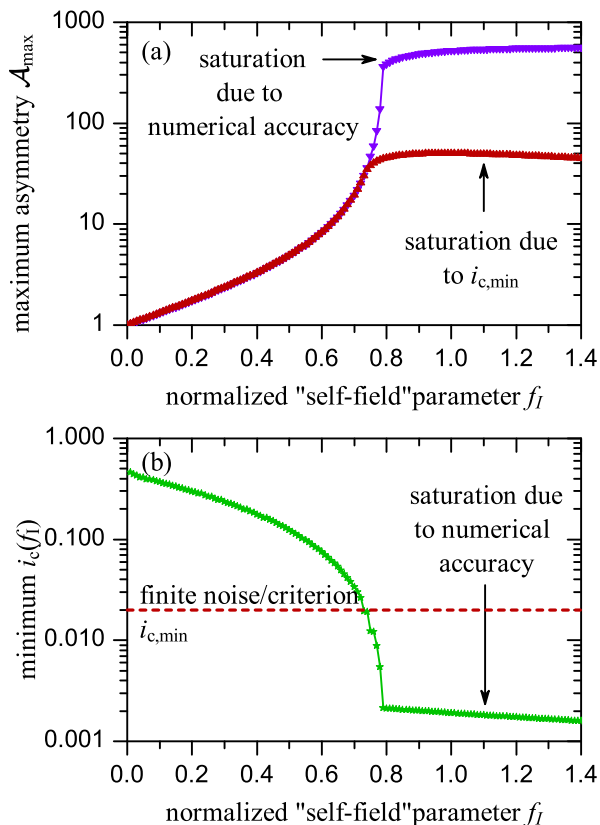


FIG. 8. (a) Maximum asymmetry parameter $\mathcal{A}_{\max}(f_I)$ taken at f_{opt} for each f_I . Violett curve is calculated according to theoretical model. Bordeaux curve is calculated taking into account that $i_{c,\min}$ cannot become smaller than 0.02. (b) The value of the minimum (by absolute value) critical current $i_{c,\min}$ at the optimal point f_{opt} as a function of f_I . Dashed line shows (as an example) the experimental limitation on $i_{c,\min}$, which then used to calculate the bordeaux curve in (a).

mum $\mathcal{A}_{\max} \equiv \mathcal{A}(f_{\text{opt}})$. Moreover, \mathcal{A}_{\max} and f_{opt} increase with increasing f_I monotonically and for $f_I \geq f_I^*$ $\mathcal{A}(f)$ develops a jump at $f = 1$ related to the discontinuity of the $i_{c+}(f)$ branch.

Finally, to see, which values of asymmetry can be reached in principle, we show $\mathcal{A}_{\max}(f_I)$ in Fig. 8(a). $\mathcal{A}_{\max}(f_I)$ rapidly increases with increasing f_I and formally diverges at f_I^* . The saturation value of $\mathcal{A}_{\max} \sim 600$ for $f_I \geq f_I^*$ is defined solely by numerical accuracy.

Thus, in the framework of the inline JJ model intro-

duced here, for optimum applied flux $f \approx 1$ and large enough in-line geometry parameter $f_I \geq f_I^*$, one can obtain almost unlimited asymmetry values.

3. Possible limitations

The model used above is an idealization. First, our initial assumption of a short JJ means that f_I defined by Eq. (B11) cannot be very large. However, we obtain very high \mathcal{A} values already for $f_I = f_I^*$. This corresponds to $L = \pi\lambda_J$, which is still within the short limit. However, the numerical solution of the sine-Gordon equation to obtain $i_c(f, f_I)$ (not presented) shows that at $L \approx (3 \dots 5)\lambda_J$ the minimum critical current does not approach zero closely, so that \mathcal{A}_{\max} just reaches values of about 5...6. Second, our approximation (linearization) of the Josephson phase in Eq. (B6) may be a reason of the extremely high \mathcal{A} obtained. The huge values of \mathcal{A} occur at $f_{\text{opt}} \approx 1$ when one of the critical currents (almost) vanishes while the other one stays finite. However, when the bias current is small, the “self-field” term (both linear and nonlinear one) plays no role for the branch with vanishing i_c . Instead, it may make a certain small correction to the branch with the high i_c . Altogether, high values of \mathcal{A} weakly depend on non-linear term in Eq. (B5).

There are several practical (experimental) limitations that do not allow one to achieve very high values of \mathcal{A} because it is very difficult experimentally to obtain vanishing $i_c(f)$ (one of the two) at f_{opt} . In Fig. 8(b) we plot the smallest critical current $|i_{c,\min}(f_I)|$ taken at f_{opt} . For $f_I \geq f_I^*$ the value of $i_{c,\min}(f_I) \sim 0.002$, which again is defined by numerical accuracy. In experiment, due to a number of reasons $i_{c,\min}$ cannot be so small. For example, (a) non-uniformity in $j_c(x)$, typical for YBCO-based JJs, results in an $i_c(f)$ pattern, where the minima are lifted relative to the $i = 0$ level. Another reason (b) is that in experiment $I_c(B)$ is measured with some finite voltage criterion V_{cr} (typically $1 \dots 2 \mu\text{V}$ due to noise and limited resolution of the equipment), which results in a background I_c level $I_c^{\text{bg}} \approx V_{\text{cr}} \cdot R_n$, where R_n is the normal resistance of the JJ. If we assume that $i_{c,\min}(f_I)$ below 0.02 cannot be measured, then the maximum value of asymmetry $\mathcal{A}_{\max} \approx 1/0.02 = 50$ at best. In Fig. 8(b), as an example, we show this level by a dashed horizontal line. If the theoretical value $i_{c\pm}(f_I)$ becomes lower, we then use 0.02 for calculation of the asymmetry \mathcal{A}_{\max} . The result is shown in Fig. 8(a) (bordeaux curve). \mathcal{A}_{\max} for $f_I \geq f_I^*$ is substantially reduced from (formally) infinity down to 40..50.

- [1] H. Linke, “Ratchets and Brownian motors: Basics, experiments and applications (editorial: introduction to special issue),” *Appl. Phys. A* **75**, 167 (2002).
 [2] P. Reimann, “Brownian motors: Noisy transport far from equilibrium,” *Phys. Rep.* **361**, 57–265 (2002).

- [3] Peter Hänggi and Fabio Marchesoni, “Artificial Brownian motors: Controlling transport on the nanoscale,” *Rev. Mod. Phys.* **81**, 387–442 (2009).
 [4] K. Svoboda, Ch. F. Schmidt, B. J. Schnapp, and S. M. Block, “Direct observation of kinesin stepping by optical

- trapping interferometry,” *Nature* **365**, 721 (1993).
- [5] F. Jülicher, A. Adjari, and J. Prost, “Modeling molecular motors,” *Rev. Mod. Phys.* **69**, 1269 (1997).
- [6] M. J. Skaug, C. Schwemmer, S. Fringes, C. D. Rawlings, and A. W. Knoll, “Nanofluidic rocking Brownian motors,” *Science* **359**, 1505–1508 (2018).
- [7] R. P. Feynman, R. B. Leighton, and M. Sands, “The feynman lectures on physics,” in *The Feynman Lectures on Physics*, Vol. I (Addison-Wesley, Reading, MA, 1966) Chap. 46 (Ratchet and Pawl).
- [8] M. Beck, E. Goldobin, M. Neuhaus, M. Siegel, R. Kleiner, and D. Koelle, “High-efficiency deterministic Josephson vortex ratchet,” *Phys. Rev. Lett.* **95**, 090603 (2005).
- [9] M. Knufinke, K. Ilin, M. Siegel, D. Koelle, R. Kleiner, and E. Goldobin, “Deterministic Josephson vortex ratchet with a load,” *Phys. Rev. E* **85**, 011122 (2012).
- [10] A. Th. A. M. de Waele and R. de Bruyn Ouboter, “Quantum-interference phenomena in point contacts between two superconductors,” *Physica* **41**, 225–254 (1969).
- [11] I. Zapata, R. Bartussek, F. Sols, and P. Hänggi, “Voltage rectification by a SQUID ratchet,” *Phys. Rev. Lett.* **77**, 2292 (1996).
- [12] S. Weiss, D. Koelle, J. Müller, R. Gross, and K. Barthel, “Ratchet effect in dc SQUIDs,” *Europhys. Lett.* **51**, 499 (2000).
- [13] A. Sterck, S. Weiss, and D. Koelle, “SQUID ratchets: Basics and experiments,” *Appl. Phys. A* **75**, 253–262 (2002).
- [14] A. Sterck, R. Kleiner, and D. Koelle, “3-junction SQUID rocking ratchet,” *Phys. Rev. Lett.* **95**, 177006 (2005).
- [15] A. Sterck, D. Koelle, and R. Kleiner, “Rectification in a stochastically driven three-junction SQUID rocking ratchet,” *Phys. Rev. Lett.* **103**, 047001 (2009).
- [16] G. Carapella and G. Costabile, “Ratchet effect: Demonstration of a relativistic fluxon diode,” *Phys. Rev. Lett.* **87**, 077002 (2001).
- [17] H. B. Wang, B. Y. Zhu, C. Gürlich, M. Ruoff, S. Kim, T. Hatano, B. R. Zhao, Z. X. Zhao, E. Goldobin, D. Koelle, and R. Kleiner, “Fast Josephson vortex ratchet made of intrinsic Josephson junctions in $\text{Bi}_2\text{Sr}_2\text{CaCu}_2\text{O}_8$,” *Phys. Rev. B* **80**, 224507 (2009).
- [18] F. Falo, P. J. Martínez, J. J. Mazo, and S. Cilla, “Ratchet potential for fluxons in Josephson-junction arrays,” *Europhys. Lett.* **45**, 700 (1999).
- [19] E. Trías, J. J. Mazo, F. Falo, and T. P. Orlando, “Depinning of kinks in a Josephson-junction ratchet array,” *Phys. Rev. E* **61**, 2257–2266 (2000), [cond-mat/9911454](#).
- [20] F. Falo, P. J. Martínez, J. J. Mazo, T. P. Orlando, K. Segall, and E. Trías, “Fluxon ratchet potentials in superconducting circuits,” *Appl. Phys. A* **75**, 263–269 (2002).
- [21] D. E. Shalóm and H. Pastoriza, “Vortex motion rectification in Josephson junction arrays with a ratchet potential,” *Phys. Rev. Lett.* **94**, 177001 (2005).
- [22] R. Menditto, H. Sickinger, M. Weides, H. Kohlstedt, D. Koelle, R. Kleiner, and E. Goldobin, “Tunable φ Josephson junction ratchet,” *Phys. Rev. E* **94**, 042202 (2016).
- [23] E. Goldobin, R. Menditto, D. Koelle, and R. Kleiner, “Model I - V curves and figures of merit of underdamped deterministic Josephson ratchets,” *Phys. Rev. E* **94**, 032203 (2016), [arXiv:1606.07371](#).
- [24] Taras Golod and Vladimir M. Krasnov, “Demonstration of a superconducting diode-with-memory, operational at zero magnetic field with switchable nonreciprocity,” *Nature Comm.* **13**, 3658 (2022).
- [25] F. Ando, Y. Miyasaka, T. Li, J. Ishizuka, T. Arakawa, Y. Shiota, T. Moriyama, Y. Yanase, and T. Ono, “Observation of superconducting diode effect,” *Nature* **584**, 373–376 (2020).
- [26] H. Narita, J. Ishizuka, R. Kawarazaki, D. Kan, Y. Shiota, T. Moriyama, Y. Shimakawa, A. V. Ognev, A. S. Samardak, Y. Yanase, and T. Ono, “Field-free superconducting diode effect in noncentrosymmetric superconductor/ferromagnet multilayers,” *Nat. Nanotechnol.* **17**, 823–828 (2022).
- [27] H. Wu, Y. Wang, Y. Xu, P. K. Sivakumar, C. Pasco, U. Filippozzi, S. S. P. Parkin, Yu.-J. Zeng, T. McQueen, and M. N. Ali, “The field-free Josephson diode in a van der Waals heterostructure,” *Nature* **604**, 653–656 (2022).
- [28] Kun-Rok Jeon, Jae-Keun Kim, Jiho Yoon, Jae-Chun Jeon, Hyeon Han, Audrey Cottet, Takis Kontos, and Stuart S. P. Parkin, “Zero-field polarity-reversible Josephson supercurrent diodes enabled by a proximity-magnetized Pt barrier,” *Nature Mat.* **21**, 1008–1013 (2022).
- [29] Banabir Pal, Anirban Chakraborty, Pranava K. Sivakumar, Margarita Davydova, Ajesh K. Gopi, Avanindra K. Pandeya, Jonas A. Krieger, Yang Zhang, Mihir Date, Sailing Ju, Noah Yuan, Niels B. M. Schröter, Liang Fu, and Stuart S. P. Parkin, “Josephson diode effect from cooper pair momentum in a topological semimetal,” *Nat. Phys.* **18**, 1228–1233 (2022).
- [30] Christian Baumgartner, Lorenz Fuchs, Andreas Costa, Simon Reinhardt, Sergei Gronin, Geoffrey C. Gardner, Tyler Lindemann, Michael J. Manfra, Paulo E. Faria Junior, Denis Kochan, Jaroslav Fabian, Nicola Paradiso, and Christoph Strunk, “Supercurrent rectification and magnetochiral effects in symmetric Josephson junctions,” *Nat. Nanotechnol.* **17**, 39–44 (2022).
- [31] F. Paolucci, G. De Simoni, and F. Giazotto, “A gate- and flux-controlled supercurrent diode effect,” *Appl. Phys. Lett.* **122**, 042601 (2023).
- [32] Sanat Ghosh, Vilas Patil, Amit Basu, Kuldeep, Achintya Dutta, Digambar A. Jangade, Ruta Kulkarni, A. Thamizhavel, Jacob F. Steiner, Felix von Oppen, and Mandar M. Deshmukh, “High-temperature Josephson diode,” *Nat. Mater.* **23**, 612–618 (2024).
- [33] Pavel A. Volkov, Étienne Lantagne-Hurtubise, Tarun Tummuru, Stephan Plugge, J. H. Pixley, and Marcel Franz, “Josephson diode effects in twisted nodal superconductors,” *Phys. Rev. B* **109**, 094518 (2024).
- [34] V. M. Krasnov, V. A. Oboznov, and N. F. Pedersen, “Fluxon dynamics in long Josephson junctions in the presence of a temperature gradient or spatial nonuniformity,” *Phys. Rev. B* **55**, 14486–14498 (1997).
- [35] A. Barone and G. Paternò, *Physics and Application of the Josephson Effect* (John Wiley and Sons, New York, 1982).
- [36] H. Kinder, P. Berberich, W. Prusseit, S. Rieder-Zecha, R. Semerad, and B. Utz, “YBCO film deposition on very large areas up to $20 \times 20 \text{ cm}^2$,” *Physica C* **282–287**, 107–110 (1997).
- [37] Shane A. Cybart, E. Y. Cho, T. J. Wong, Björn H. Wehlin, Meng K. Ma, Chuong Huynh, and R. C. Dynes, “Nano Josephson superconducting tunnel junctions in $\text{YBa}_2\text{Cu}_3\text{O}_{7-\delta}$ directly patterned with a focused helium

- ion beam,” *Nature Nanotechnol.* **10**, 598 (2015).
- [38] E. Y. Cho, Y. W. Zhou, J. Y. Cho, and S. A. Cybart, “Superconducting nano Josephson junctions patterned with a focused helium ion beam,” *Appl. Phys. Lett.* **113**, 022604 (2018).
- [39] B. Müller, M. Karrer, F. Limberger, M. Becker, B. Schröppel, C. J. Burkhardt, R. Kleiner, E. Goldobin, and D. Koelle, “Josephson junctions and SQUIDs created by focused helium-ion-beam irradiation of $\text{YBa}_2\text{Cu}_3\text{O}_7$,” *Phys. Rev. Appl.* **11**, 044082 (2019).
- [40] M. Karrer, K. Wurster, J. Linek, M. Meichsner, R. Kleiner, E. Goldobin, and D. Koelle, “Temporal evolution of electric transport properties of $\text{YBa}_2\text{Cu}_3\text{O}_{7-\delta}$ Josephson junctions produced by focused-helium-ion-beam irradiation,” *Phys. Rev. Appl.* **21**, 014065 (2024).
- [41] R. Hutt, C. Magén, *et al.*, unpublished.
- [42] C. Guarcello, S. Pagano, and G. Filatrella, “Efficiency of diode effect in asymmetric inline long Josephson junctions,” *Appl. Phys. Lett.* **124**, 162601 (2024).
- [43] T. Golod, O.M. Kapran, and V.M. Krasnov, “Planar superconductor-ferromagnet-superconductor Josephson junctions as scanning-probe sensors,” *Phys. Rev. Appl.* **11**, 014062 (2019).
- [44] R. Gerdemann, T. Bauch, O. M. Fröhlich, L. Alff, A. Beck, D. Koelle, and R. Gross, “Asymmetric high temperature superconducting Josephson vortex-flow transistors with high current gain,” *Appl. Phys. Lett.* **67**, 1010–1012 (1995).
- [45] T. Bauch, S. Weiss, H. Haensel, A. Marx, D. Koelle, and R. Gross, “High-temperature superconducting Josephson vortex flow transistors: numerical simulations and experimental results,” *IEEE Trans. Appl. Supercond.* **7**, 3605–3608 (1997).
- [46] V. G. Kogan, V. V. Dobrovitski, J. R. Clem, Yasunori Mawatari, and R. G. Mints, “Josephson junction in a thin film,” *Phys. Rev. B* **63**, 144501 (2001).
- [47] In Ref. 9, only \bar{V} was measured. From Fig. 2 and Fig. 3, we determine that $I_{c-} = -0.5$ and $I_{c+} = 0.3$ in units of $I_0 = 2.8 \text{ mA}$. We then find $I_{dc}^{opt} \approx -0.06$ corresponds to maximum \bar{P}_{out} from eq. (18), and substitute this value in eq. (17) to obtain maximum \bar{P}_{out} . Note that, the quantities in eq. (17) are normalized. Therefore, to obtain the power in physical units, we multiply by $V_1 \cdot I_0 = 280 \text{ nW}$, where $V_1 \approx 100 \mu\text{V}$.
- [48] The value of efficiency was not measured experimentally but instead it is *calculated* by us from the experimentally reported asymmetry using the expression (11).
- [49] Quoted asymmetry and other figures of merit are given for zero magnetic field. At the optimum magnetic field the asymmetry ~ 10 .
- [50] The authors used rectangular drive. For sine-drive the average voltage will be (substantially) lower.
- [51] R. Bartussek, P. Hänggi, and J. G. Kissner, “Periodically rocked thermal ratchets,” *Europhys. Lett.* **28**, 459–464 (1994).
- [52] According to the RSJ-like model[9] the linear rectification branch should start at I_{c+} and the maximum of the $\bar{V}(I_{ac})$ curve should appear exactly at I_{c+} . However, in Fig. 3(a) the $\bar{V}(I_{ac})$ curves seem to be shifted somewhat to the right relative to I_{c+} and I_{c-} . This is related to the rounding of our IVC near I_{c+} and I_{c-} , which is not captured by the model[9]. Namely, the value of the current I_{m+} , where the differential resistance reaches its maximum, is somewhat larger than I_{c+} . Similarly, $|I_{m-}| \gtrsim |I_{c-}|$. Thus, at $I_{ac} = I_{c+}$ we do have the onset of rectification, however the voltage becomes substantial (linear branch starts) at $I_{ac} > I_{m+}$. Similarly, at $I_{ac} = |I_{c-}|$ the rectification curve starts bending down, but its maximum is reached at $|I_{m+}|$. In the RSJ-like IVC of the model[9] $I_{m\pm} = I_{c\pm}$.
- [53] Formally, rectification takes place in an infinite range of $I_{ac} = I_{c+} \dots \infty$ where $\bar{V} > 0$. However, for $I_{ac} > |I_{c-}|$ the ratchet works in the so-called “Sisyphus regime”, where the particle moves in the asymmetric potential back and forth, dissipating a lot with a little net progress. Instead, for $I_{c+} < I_{ac} < |I_{c-}|$ the particle moves only in the easy (positive) direction and is blocked in the difficult (difficult) direction.
- [54] In a tri-layer (strip-line) geometry, ℓ_J is known as “inductance per square” of superconducting (thin film) electrodes forming the JJ.